Parametric Net Influx Rate Images of ^{68}Ga-DOTATOC and ^{68}Ga-DOTATATE: Quantitative Accuracy and Improved Image Contrast

Ezgi Ilan[1,2], Mattias Sandström[1,2], Irina Velikyan[1,3], Anders Sundin[1,3], Barbro Eriksson[4], and Mark Lubberink[1,2]

[1]Section of Nuclear Medicine and PET, Department of Surgical Sciences, Uppsala University, Uppsala, Sweden; [2]Medical Physics, Uppsala University Hospital, Uppsala, Sweden; [3]PET-Centre, Medical Imaging Centre, Uppsala University Hospital, Uppsala, Sweden; and [4]Section of Endocrine Oncology, Department of Medical Science, Uppsala University Hospital, Uppsala, Sweden

^{68}Ga-DOTATOC and ^{68}Ga-DOTATATE are radiolabeled somatostatin analogs used for the diagnosis of somatostatin receptor–expressing neuroendocrine tumors (NETs), and SUV measurements are suggested for treatment monitoring. However, changes in net influx rate (K_i) may better reflect treatment effects than those of the SUV, and accordingly there is a need to compute parametric images showing K_i at the voxel level. The aim of this study was to evaluate parametric methods for computation of parametric K_i images by comparison to volume of interest (VOI)–based methods and to assess image contrast in terms of tumor-to-liver ratio. **Methods:** Ten patients with metastatic NETs underwent a 45-min dynamic PET examination followed by whole-body PET/CT at 1 h after injection of ^{68}Ga-DOTATOC and ^{68}Ga-DOTATATE on consecutive days. Parametric K_i images were computed using a basis function method (BFM) implementation of the 2-tissue-irreversible-compartment model and the Patlak method using a descending aorta image–derived input function, and mean tumor K_i values were determined for 50% isocontour VOIs and compared with K_i values based on nonlinear regression (NLR) of the whole-VOI time–activity curve. A subsample of healthy liver was delineated in the whole-body and K_i images, and tumor-to-liver ratios were calculated to evaluate image contrast. Correlation (R^2) and agreement between VOI-based and parametric K_i values were assessed using regression and Bland–Altman analysis. **Results:** The R^2 between NLR-based and parametric image–based (BFM) tumor K_i values was 0.98 (slope, 0.81) and 0.97 (slope, 0.88) for ^{68}Ga-DOTATOC and ^{68}Ga-DOTATATE, respectively. For Patlak analysis, the R^2 between NLR-based and parametric-based (Patlak) tumor K_i was 0.95 (slope, 0.71) and 0.92 (slope, 0.74) for ^{68}Ga-DOTATOC and ^{68}Ga-DOTATATE, respectively. There was no bias between NLR and parametric-based K_i values. Tumor-to-liver contrast was 1.6 and 2.0 times higher in the parametric BFM K_i images and 2.3 and 3.0 times in the Patlak images than in the whole-body images for ^{68}Ga-DOTATOC and ^{68}Ga-DOTATATE, respectively. **Conclusion:** A high R^2 and agreement between NLR- and parametric-based K_i values was found, showing that K_i images are quantitatively accurate. In addition, tumor-to-liver contrast was superior in the parametric K_i images compared with whole-body images for both ^{68}Ga-DOTATOC and ^{68}Ga DOTATATE.

Key Words: ^{68}Ga-DOTATOC; ^{68}Ga-DOTATATE; parametric images; net influx rate; neuroendocrine tumors

J Nucl Med 2017; 58:744–749
DOI: 10.2967/jnumed.116.180380

Neuroendocrine tumors (NETs) are tumors derived from the disseminated system of endocrine cells in the body and have diverse biologic and clinical characteristics (*1*). Epidemiologic studies have shown that the NET incidence is rising, and according to an analysis of the North American Surveillance, Epidemiology, and End Results registry data the annual age-adjusted incidence increased from 1.09/100,000 in 1973 to 5.25/100,000 in 2004. The reason for this is assumed to be the improvements in imaging technology (*2*).

NETs are characterized by cellular overexpression of somatostatin receptors (SSTRs), allowing for the use of unlabeled and radiolabeled somatostatin analogs (SSAs) for imaging and therapy. SSTR scintigraphy with the ^{111}In-labeled SSA ^{111}In-DTPA-octreotide (OctreoScan; Mallinckrodt Inc.) remains the mainstay for functional NET imaging and continues to play an important role for NET imaging (*3,4*). However, PET using ^{68}Ga-labeled SSAs, such as ^{68}Ga-DOTATOC, ^{68}Ga-DOTANOC, and ^{68}Ga-DOTATATE, is gradually replacing SSTR scintigraphy and is expected to become the future gold standard for SSTR imaging of NETs (*5*). PET/CT with ^{68}Ga-SSA shows a specificity and sensitivity well above 90%, exceeding that of OctreoScan and CT (*6–11*).

In disseminated disease, unlabeled SSA constitutes first-line therapy for low-grade NETs. During the last decade, peptide receptor radionuclide therapy (PRRT), with radiolabeled SSAs such as ^{177}Lu-DOTATATE and ^{90}Y-DOTATOC, has been shown to be effective and plays an increasingly important role in the treatment of NET patients (*12–21*). However, large interpatient variability in organ distribution and consequently radiation dose delivered to the lesions and normal organs calls for the development of methods for individualized radiotherapy planning (*22*). Conventional radiologic imaging techniques such as CT and MRI are well established for the evaluation of therapy response in the clinical routine by assessing changes in tumor size and diagnosing new lesions. The RECIST (*23*), are, however, not optimal to monitor systemic NET therapies because tumor shrinkage is seen only in a small fraction of patients and instead the treatments mainly induce tumor stabilization.

Received Jun. 29, 2016; revision accepted Oct. 4, 2016.
For correspondence or reprints contact: Ezgi Ilan, Uppsala University Hospital, Medical Physics, SE-751 85 Uppsala, Sweden.
E-mail: ezgi.ilan@akademiska.se
Published online Oct. 27, 2016.

Moreover, PRRT induces long-time effects due to β-emission of ^{177}Lu and ^{90}Y, resulting in continuously increasing necrosis and decrease of viable tumor although the tumor size may appear unchanged during the subsequent examinations (*24*). Also, with the new so-called targeted therapies tumor shrinkage is less common and the heterogeneous nature of tumors also adds uncertainty to such measurements. There is therefore a need for new methods to evaluate NET therapy response besides conventional morphologic size criteria (*25*).

In parallel with the increasing use of ^{18}F-FDG PET/CT for therapy monitoring in conventional oncology, this application has also been suggested for NETs. However, because of the low proliferation and low metabolic activity of NET cells, they are generally not ^{18}F-FDG–avid (*26*). By contrast, most NETs express SSTRs and show high ^{68}Ga-SSA uptake. Consequently, ^{68}Ga-DOTATOC and ^{68}Ga-DOTATATE have been tested to assess NET therapy response (*6,24,27*). In 1 study (*24*), the authors found that the changes in tumor SUV between baseline and follow-up ^{68}Ga-DOTATOC PET/CT did not correlate to the outcome of PRRT. This was also found in another study (*27*), although changes in the tumor-to-spleen SUV ratio between baseline and follow-up ^{68}Ga-DOTATOC were shown to be more accurate than changes in tumor SUV_{max} to evaluate the response to PRRT. The problems of applying static tumor uptake measurements in these 2 therapy monitoring studies may be explained, at least partly, by the results in a recent study (*6*) on ^{68}Ga-DOTATOC and ^{68}Ga-DOTATATE. In this study, SUV saturated at a static value for high net uptake rate (K_i), especially for higher SUVs (>20–25). Hence, SUV does not appear to reflect SSTR density for tumors with high receptor expression. Consequently, changes in K_i may better reflect treatment response than changes in SUV.

To facilitate the clinical use of K_i, accurate and reliable computation of parametric images showing K_i at the voxel level is desirable. Moreover, information on K_i at the voxel level provides information on tumor heterogeneity that is lost when average tumor K_i is assessed. The aim of this study was to evaluate methods for computation of parametric K_i images by comparison to volume of interest (VOI)–based methods. A secondary aim was to explore the conditions for lesion detection in K_i images by assessing the image contrast in terms of tumor-to-liver ratios compared with those in static SUV images.

MATERIALS AND METHODS

Patients

Ten patients (6 men and 4 women; mean age ± SD, 65 ± 10 y) diagnosed with disseminated gastroenteropancreatic NETs, confirmed by histopathology, were included in the study. Five patients had small-intestinal NETs, 3 had pancreatic NETs, and 2 had lung carcinoids. The total number of tumors included in the study was 16; 5 patients had 1 tumor, 1 patient had 2 tumors, and 3 patients had 3 tumors. Only tumors with a diameter of more than 1 cm and high uptake (determined visually) were included. The study was approved by the Regional Ethical Review Board in Uppsala and the Radiation Ethics Committee at Uppsala University Hospital, and all patients signed a written informed consent form before inclusion in the study.

Image Acquisition and Reconstruction

Each patient underwent a ^{68}Ga-DOTATOC and ^{68}Ga-DOTATATE PET/CT examination on consecutive days, in random order. The patients received a bolus injection of 86.9 ± 16.4 MBq (range, 61–113 MBq) of ^{68}Ga-DOTATOC and 91.4 ± 18.7 MBq (range, 67–121 MBq) of ^{68}Ga-DOTATATE. Good manufacturing practice–compliant production of ^{68}Ga-DOTATOC and ^{68}Ga-DOTATATE was accomplished as previously described (*6,28*).

Images were acquired on a Discovery ST PET/CT scanner (GE Healthcare) with a transaxial and axial field of view of 70 and 15.7 cm, respectively. The image matrix size was 128 × 128, with a voxel size of 3.9 × 3.9 × 3.27 mm. The patients underwent a low-dose CT scan (140 kV; auto mA; 20–80 mA) followed by a 45-min dynamic PET examination of the abdomen to include the major tumor load. The dynamic PET examination started simultaneously with the intravenous injection of ^{68}Ga-DOTATOC or ^{68}Ga-DOTATATE and consisted of 22 time frames of increasing durations (6 × 10, 3 × 20, 3 × 60, 5 × 180, and 5 × 300 s). The dynamic examination was followed by a whole-body PET/CT scan ranging from the proximal femur to the base of the skull (3 min per bed position) starting at 60 min after injection after a second low-dose CT for attenuation correction of the whole-body images. Peripheral venous blood samples (~1 mL) were taken at 5, 20, 45, and 60 min after injection to assess the whole-blood and plasma radioactivity concentrations, respectively. The PET data were normalized and corrected for dead time, random coincidences, scatter, and attenuation and were reconstructed using ordered-subsets expectation maximization with 2 iterations and 21 subsets applying a 5.4-mm gaussian postprocessing filter.

Image-Derived Input Functions

Because labeling with ^{68}Ga-DOTATOC/DOTATATE is stable during the duration of the PET examination, the total radioactivity concentration in the arterial plasma was used as an input function (*6*). Circular regions of interest with a diameter of 1 cm were drawn over the descending aorta in 10 consecutive image planes in the time frame in which the first passage of the bolus was best visualized (typically frame 1–10). These regions of interest were then combined to form a single aortic VOI. The resulting aortic VOI was projected onto all time frames in the dynamic examination to produce an arterial time–activity curve. The image-derived input functions were calculated by multiplying the arterial time–activity curve with the mean plasma–to–whole blood ratio in venous blood (*29,30*).

VOI-Based Kinetic Analysis

Fifty percent isocontour tumor VOIs were drawn in the 20- to 45-min summation image of the dynamic data and were projected onto all time frames to generate tumor time–activity curves, using the NEDPAS software developed at VU University Medical Centre (Amsterdam) (*31*). The tumors were delineated similarly in the whole-body images, and the corresponding tumor SUVs were derived. To evaluate the tumor-to-liver contrast, a subsample of healthy liver was delineated in the whole-body images using a spheric 20-mL VOI.

It has previously been shown that the kinetics of ^{68}Ga-DOTATOC/DOTATATE can be described by an irreversible 2-tissue-compartment model (*32–36*), which reflects internalization of the receptor–ligand complex. From this compartment model, the following differential equations can be defined:

$$\frac{dC_1(t)}{dt} = K_1 C_P(t) - (k_2 + k_3) C_1(t), \qquad \text{Eq. 1}$$

where $C_1(t)$ is the concentration of free tracer in tissue; $C_P(t)$ is the concentration in plasma; K_1, k_2, and k_3 are rate constants; and:

$$\frac{dC_2(t)}{dt} = k_3 C_1(t), \qquad \text{Eq. 2}$$

where $C_2(t)$ is the concentration of tracer internalized into the tumor cell. The solution of this model, with the addition of a blood volume component, is given by the following equation:

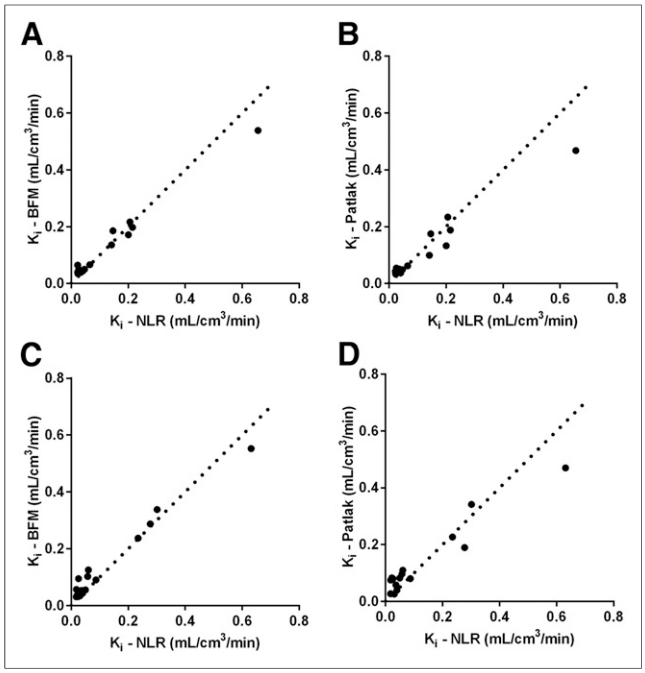

FIGURE 1. Correlation between NLR- and parametric-based (BFM and Patlak) K_i values for ^{68}Ga-DOTATOC (A and B) and ^{68}Ga-DOTATATE (C and D). Dashed lines represent lines of identity.

$$C_{PET}(t) = (K_1 - K_i)e^{-(k_2+k_3)t} \otimes C_P(t) + K_i \otimes C_P(t) + V_A C_A(t), \quad \text{Eq. 3}$$

in which $C_{PET}(t)$ represents the measured concentration, V_A the arterial blood volume, $C_A(t)$ the arterial blood concentration, and K_i the net uptake rate (*37*) defined as:

$$K_i = \frac{K_1 k_3}{k_2 + k_3}. \quad \text{Eq. 4}$$

By fitting Equation 3 to the measured PET data using nonlinear regression (NLR), K_i can be determined, which is assumed to reflect a combination of receptor density and the ability of the ligand to internalize in the tumors (*6*).

Parametric Image Analysis

Parametric K_i images were generated first by a basis function method (BFM) implementation of the irreversible 2-tissue-compartment model (*38,39*) and second by application of the Patlak method (*37,40*) (t* = 15 min after injection) on the dynamic PET data 15–45 min after injection, using in-house–developed software in MATLAB. For the BFM implementation, 20 logarithmically spaced exponential clearance rates ($\alpha = k_2 + k_3$) ranging between 0.1 and 0.8 min^{-1} were used in addition to an irreversible basis function to create a set of basis functions:

$$BF_i = e^{-\alpha_i t} \otimes C_P(t). \quad \text{Eq. 5}$$

The linear combination of the 3 terms in Equation 3, using BF_i that resulted in the minimum sum of squared residuals, yielded K_1-K_i, K_i, and V_A for each voxel. Before parametric computations, a gaussian filter with a full width at half maximum of 5 mm was applied. Mean tumor K_i values were determined for 50% isocontour VOIs in the parametric images. Liver VOIs were drawn in the parametric K_i images (as described above for the whole-body images), and tumor-to-liver ratios were calculated.

Statistical Analysis

The agreement and correlation between the VOI-based and parametric-based K_i values were determined using Pearson correlation, Deming regression, and Bland–Altman analysis (Prism, version 6.04; GraphPad Software, Inc.).

RESULTS

VOI- and Parametric-Based Kinetic Analysis

A linear relation was found between the VOI-based and parametric-based K_i values for both ^{68}Ga-DOTATOC and ^{68}Ga-DOTATATE. The relations between the VOI-based (NLR) and parametric-based (BFM and Patlak) K_i values for ^{68}Ga-DOTATOC and ^{68}Ga-DOTATATE are shown in Figure 1. Pearson correlation coefficients, Deming regression slope, and bias for the VOI- (NLR) and parametric-based (BFM and Patlak) K_i are listed in Table 1. For both tracers, the Pearson correlation coefficient was higher for BFM than for Patlak, the slope of regression line was higher for BFM than for Patlak (Table 1), and no significant bias was found for either parametric method or tracer.

Parametric K_i values determined by BFM and Patlak for ^{68}Ga-DOTATOC and ^{68}Ga-DOTATATE are illustrated in Figures 2A and 2B, respectively. The Pearson correlation coefficient between BFM and Patlak *K*i values was 0.99 for ^{68}Ga-DOTATOC and 0.98 for ^{68}Ga-DOTATATE. The Deming regression line slope between BFM and Patlak *K*i values was 0.88 for ^{68}Ga-DOTATOC and 0.85 for ^{68}Ga-DOTATATE. The bias from the Bland–Altman plots was 0.01 (95% confidence interval, −0.05 to 0.03) and 0.01 (95% confidence interval, −0.08 to 0.06) for ^{68}Ga-DOTATOC and ^{68}Ga-DOTATATE, respectively.

TABLE 1
Pearson Correlation Coefficients (R^2), Deming Regression Slope, and Bias Between Tumor VOI (NLR) and Parametric-Based (BFM and Patlak) K_i Values

SSA	Method	Correlation (R^2)	Slope	Bias
^{68}Ga-DOTATOC	BFM	0.98	0.81 (0.75 to 0.87)	0.00 (−0.07 to 0.07)
	Patlak	0.95	0.71 (0.62 to 0.80)	0.00 (−0.12 to 0.10)
^{68}Ga-DOTATATE	BFM	0.97	0.88 (0.79 to 0.96)	0.02 (−0.05 to 0.08)
	Patlak	0.92	0.74 (0.62 to 0.86)	0.00 (−0.11 to 0.12)

Data in parentheses are 95% confidence intervals.

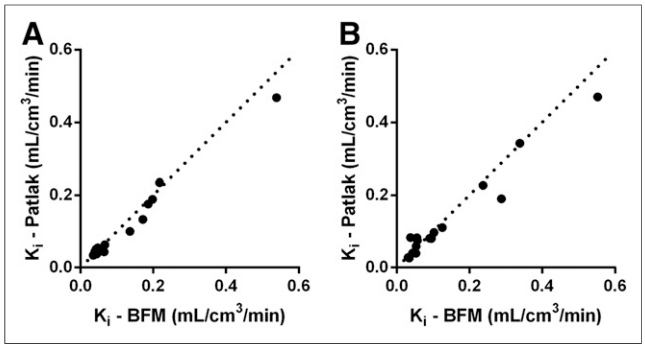

FIGURE 2. Correlation between parametric K_i in tumor VOIs determined by BFM and Patlak analysis for ^{68}Ga-DOTATOC (A) and ^{68}Ga-DOTATATE (B). Dashed lines represent line of identity.

Tumor-to-Liver Contrast

The image contrast visually improved in the parametric K_i images for both ^{68}Ga-DOTATOC and ^{68}Ga-DOTATATE (Fig. 3), and the tumor-to-liver ratio was generally higher in the parametric K_i images than in the whole-body images (Fig. 4). The tumor-to-liver ratio was 1.6 and 2.0 times higher in the parametric K_i images based on BFM than in the whole-body images for ^{68}Ga-DOTATOC and ^{68}Ga-DOTATATE (Fig. 4A), respectively. For the parametric K_i images based on the Patlak method, the tumor-to-liver ratio was 2.3 and 3.0 times higher than in the whole-body images for ^{68}Ga-DOTATOC and ^{68}Ga-DOTATATE (Fig. 4B), respectively. Generally, the image contrast was higher for ^{68}Ga-DOTATATE than for ^{68}Ga-DOTATOC (Fig. 4).

DISCUSSION

Early prediction of treatment response is essential to guide tumor therapy and avoid unnecessary side effects and costs from ineffective treatments. SUV has been proposed as a marker of SSTR density but changes of tumor SUV at ^{68}Ga-DOTATOC PET/CT during PRRT have not been found to reliably correlate with the patient outcome (*24,27,41–43*). It was previously shown that K_i and SUV are not linearly correlated for NETs (especially for higher SUVs $>$ 20–25), and the former may more adequately reflect the tumor SSTR density than SUV (*6*). However, in the present study, k_3 was found to be much higher than k_2 in patients with high K_i, indicating flow-limited delivery and an associated underestimation of both K_i and SUV, so this cannot explain the previously observed divergence between K_i and SUV. A more detailed analysis showed that the difference between SUV and K_i can rather be attributed to faster plasma clearance in patients with a high receptor burden, because the plasma radioactivity concentration at 45 min after injection in patients with high K_i values was considerably lower than in patients with low K_i values. This, in turn, would not affect the accuracy of K_i because plasma concentrations are considered when estimating K_i, but it does affect SUV because the absolute amount of tracer taken up into tissue is limited by the low plasma activity concentrations. Possibly, the total number of receptors in these patients is so high that nearly all peptide is cleared from the plasma during the scan, leading to the apparent saturation of SUVs.

The primary aim of this study was to develop a method to compute images that would incorporate the K_i parameter, allowing a more accurate determination of receptor density as well as a comparison of NLR- and parametric-based K_i values. Two sets of parametric K_i values were accordingly generated, and we presented a comparison between NLR-based and parametric-based K_i values for ^{68}Ga-DOTATOC and ^{68}Ga-DOTATATE. In a subset of 10 patients with 16 tumors, high correlation and agreement were found between the VOI- and parametric-based K_i values (Fig. 1), and no significant bias was found for the 2 methods, neither for ^{68}Ga-DOTATOC nor for ^{68}Ga-DOTATATE. Consequently, BFM and Patlak methods for computation of parametric images performed equally well and produced similar K_i values for both ^{68}Ga-DOTATOC and ^{68}Ga-DOTATATE. The agreement and correlation between the 2 parametric methods (BFM and Patlak) were also tested, and both methods were found to generate similar K_i values. However, parametric images appeared to show a considerable overestimation for low K_i values and a slight underestimation for high K_i values compared with NLR (Supplemental Figs. 1 and 2; supplemental materials are available at http://jnm.snmjournals.org). A possible explanation for this is that for low tumor uptake, the time–activity curves obtained from the 50% VOI in the dynamic images are a combination of the actual tumor uptake and spill-in from surrounding tissue. Because K_i in the surrounding liver tissue is much lower than in tumor tissue, VOI-based analysis using NLR will probably underestimate tumor K_i values. Because the liver background in the parametric images is much lower, the K_i values derived from the parametric images will to a much larger extent represent the actual tumor K_i and thus will be higher than the NLR values. In addition, VOIs were drawn independently in parametric and whole-body images. However, using the same VOIs in the dynamic and parametric images did not

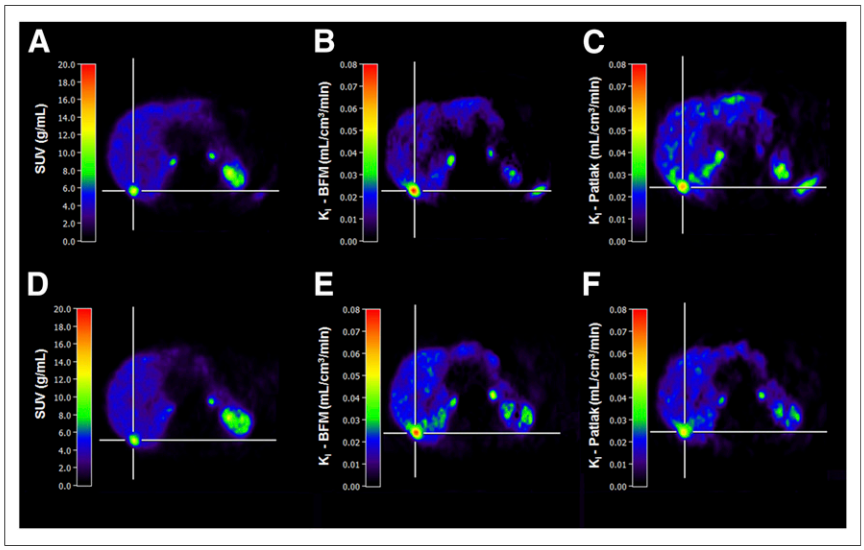

FIGURE 3. Representative transaxial images of liver obtained from static whole-body examination at 1 h after injection (A: ^{68}Ga-DOTATOC; D: ^{68}Ga-DOTATATE) and parametric K_i images based on BFM (B: ^{68}Ga-DOTATOC; E: ^{68}Ga-DOTATATE) and Patlak method (C: ^{68}Ga-DOTATOC; F: ^{68}Ga-DOTATATE), showing comparison of image contrast.

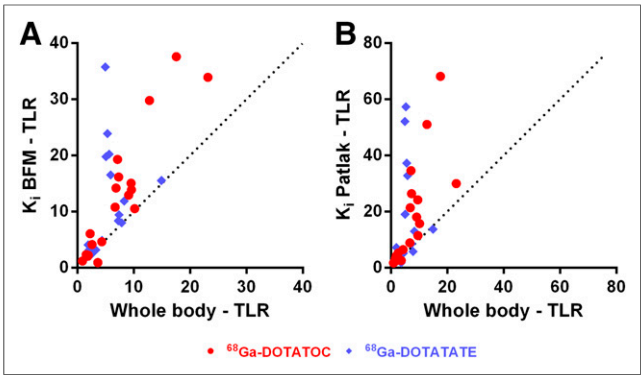

FIGURE 4. Tumor-to-liver ratio (TLR) for whole-body and parametric K_i images for BFM (A) and Patlak (B) both for ^{68}Ga-DOTATOC and ^{68}Ga-DOTATATE. Dashed lines represent lines of identity. Mean tumor to liver contrasts were 1.6 (A, red dot), 2.0 (A, blue diamond), 2.3 (B, red dot), and 3.0 (B, blue diamond) times higher in parametric K_i images than in whole-body images.

alter the conclusion—that is, parametric K_i values remained higher than NLR-based K_i values.

Many NET patients develop liver metastases but, because of the moderately high physiologic liver uptake of ^{68}Ga-DOTATOC/DOTATATE, the detection of liver lesions may be jeopardized, especially when they are small. Also, this makes it challenging to evaluate therapy response because the physiologic liver background will affect the accuracy of the tumor uptake measurements. The tumor-to-liver ratios for whole-body SUV and parametric K_i images were therefore compared, and the latter were found to provide considerably better image contrast for both tracers (Figs. 3 and 4), although this was most apparent for ^{68}Ga-DOTATATE. As previously shown (*6*), the uptake of ^{68}Ga-DOTATOC/DOTATATE in both liver and tumors is more or less constant from 40 min after injection, with a possible small continuing increase for tumors. Therefore, using other uptake times for the SUV image in this comparison would not have affected contrast, but noise would increase for later time points. Consequently, the parametric K_i images can additionally be used to better visualize liver metastases. However, for its clinical implementation, automated methods for image-derived input function definition, such as previously presented, for example, for ^{15}O-water myocardial blood flow imaging (*44*), need to be developed.

Because of the dynamic acquisition protocol required to generate the parametric K_i images, the whole abdomen or thorax may not be included for examination. The anatomic region that may be included for examination is therefore limited to the 15.5-cm axial field of view of the current PET/CT system, which reduces the clinical usefulness of the method. However, the recent generation of PET/CT and PET/MRI scanners, providing up to a 25-cm axial field of view, is a considerable improvement in this respect. Also, an alternative acquisition protocol may be applied to generate whole-body parametric Patlak K_i images, based on a short dynamic scan over the thorax followed by fast serial whole-body scanning. This alternative acquisition protocol will be the subject of future work.

CONCLUSION

Quantitatively accurate parametric K_i images, showing K_i of ^{68}Ga-DOTATOC or ^{68}Ga-DOTATATE at the voxel level, can be computed using the methods presented in the present work. In addition, the parametric methods reduced the signal from the liver for both tracers, providing better tumor-to-liver contrast in the parametric K_i images than in whole-body images. Further methodologic developments are necessary for clinical implementation of parametric K_i images to be feasible.

DISCLOSURE

No potential conflict of interest relevant to this article was reported.

ACKNOWLEDGMENTS

We express our gratitude to Mimmi Lindholm, Annie Bjurebäck, Maj Wiberg, Lars Lindsjö, and Marie Åhlman for their assistance in the PET/CT examinations.

REFERENCES

1. Sundin A, Rockall A. Therapeutic monitoring of gastroenteropancreatic neuroendocrine tumors: the challenges ahead. *Neuroendocrinology.* 2012;96:261–271.
2. Yao JC, Hassan M, Phan A, et al. One hundred years after "carcinoid": epidemiology of and prognostic factors for neuroendocrine tumors in 35,825 cases in the United States. *J Clin Oncol.* 2008;26:3063–3072.
3. Bodei L, Pepe G, Paganelli G. Peptide receptor radionuclide therapy (PRRT) of neuroendocrine tumors with somatostatin analogues. *Eur Rev Med Pharmacol Sci.* 2010;14:347–351.
4. Bodei L, Mueller-Brand J, Baum RP, et al. The joint IAEA, EANM, and SNMMI practical guidance on peptide receptor radionuclide therapy (PRRNT) in neuroendocrine tumours. *Eur J Nucl Med Mol Imaging.* 2013;40:800–816.
5. van Essen M, Sundin A, Krenning EP, Kwekkeboom DJ. Neuroendocrine tumours: the role of imaging for diagnosis and therapy. *Nat Rev Endocrinol.* 2014;10:102–114.
6. Velikyan I, Sundin A, Sorensen J, et al. Quantitative and qualitative intrapatient comparison of ^{68}Ga-DOTATOC and ^{68}Ga-DOTATATE: net uptake rate for accurate quantification. *J Nucl Med.* 2014;55:204–210.
7. Al-Nahhas A. Nuclear medicine imaging of neuroendocrine tumours. *Clin Med (Lond).* 2012;12:377–380.
8. Öberg K. Gallium-68 somatostatin receptor PET/CT: is it time to replace ^{111}Indium DTPA octreotide for patients with neuroendocrine tumors? *Endocrine.* 2012;42:3–4.
9. Schreiter NF, Brenner W, Nogami M, et al. Cost comparison of ^{111}In-DTPA-octreotide scintigraphy and ^{68}Ga-DOTATOC PET/CT for staging enteropancreatic neuroendocrine tumours. *Eur J Nucl Med Mol Imaging.* 2012;39:72–82.
10. Gabriel M, Decristoforo C, Kendler D, et al. ^{68}Ga-DOTA-Tyr3-octreotide PET in neuroendocrine tumors: comparison with somatostatin receptor scintigraphy and CT. *J Nucl Med.* 2007;48:508–518.
11. Ambrosini V, Campana D, Bodei L, et al. ^{68}Ga-DOTANOC PET/CT clinical impact in patients with neuroendocrine tumors. *J Nucl Med.* 2010;51:669–673.
12. Kam BL, Teunissen JJ, Krenning EP, et al. Lutetium-labelled peptides for therapy of neuroendocrine tumours. *Eur J Nucl Med Mol Imaging.* 2012;39(suppl 1):S103–S112.
13. Kwekkeboom DJ, Teunissen JJ, Bakker WH, et al. Radiolabeled somatostatin analog [^{177}Lu-DOTA0,Tyr3]octreotate in patients with endocrine gastroenteropancreatic tumors. *J Clin Oncol.* 2005;23:2754–2762.
14. Kwekkeboom DJ, de Herder WW, Kam BL, et al. Treatment with the radiolabeled somatostatin analog [177 Lu-DOTA 0,Tyr3]octreotate: toxicity, efficacy, and survival. *J Clin Oncol.* 2008;26:2124–2130.
15. Bergsma H, van Vliet EI, Teunissen JJ, et al. Peptide receptor radionuclide therapy (PRRT) for GEP-NETs. *Best Pract Res Clin Gastroenterol.* 2012;26:867–881.
16. Kwekkeboom DJ, Bakker WH, Kam BL, et al. Treatment of patients with gastro-entero-pancreatic (GEP) tumours with the novel radiolabelled somatostatin analogue [^{177}Lu-DOTA(0),Tyr3]octreotate. *Eur J Nucl Med Mol Imaging.* 2003;30:417–422.
17. Forrer F, Uusijarvi H, Storch D, Maecke HR, Mueller-Brand J. Treatment with ^{177}Lu-DOTATOC of patients with relapse of neuroendocrine tumors after treatment with ^{90}Y-DOTATOC. *J Nucl Med.* 2005;46:1310–1316.

18. Kwekkeboom DJ, Mueller-Brand J, Paganelli G, et al. Overview of results of peptide receptor radionuclide therapy with 3 radiolabeled somatostatin analogs. *J Nucl Med.* 2005;46(suppl 1):62S–66S.
19. Bodei L, Cremonesi M, Grana CM, et al. Peptide receptor radionuclide therapy with ^{177}Lu-DOTATATE: the IEO phase I-II study. *Eur J Nucl Med Mol Imaging.* 2011;38:2125–2135.
20. Gabriel M, Andergassen U, Putzer D, et al. Individualized peptide-related-radionuclide-therapy concept using different radiolabelled somatostatin analogs in advanced cancer patients. *Q J Nucl Med Mol Imaging.* 2010;54: 92–99.
21. Garske U, Sandstrom M, Johansson S, et al. Lessons on tumour response: imaging during therapy with ^{177}Lu-DOTA-octreotate—a case report on a patient with a large volume of poorly differentiated neuroendocrine carcinoma. *Theranostics.* 2012;2:459–471.
22. Chalkia MT, Stefanoyiannis AP, Chatziioannou SN, Round WH, Efstathopoulos EP, Nikiforidis GC. Patient-specific dosimetry in peptide receptor radionuclide therapy: a clinical review. *Australas Phys Eng Sci Med.* 2015;38:7–22.
23. Eisenhauer EA, Therasse P, Bogaerts J, et al. New response evaluation criteria in solid tumours: revised RECIST guideline (version 1.1). *Eur J Cancer.* 2009;45: 228–247.
24. Gabriel M, Oberauer A, Dobrozemsky G, et al. ^{68}Ga-DOTA-Tyr3-octreotide PET for assessing response to somatostatin-receptor-mediated radionuclide therapy. *J Nucl Med.* 2009;50:1427–1434.
25. Oberg K, Jelic S, Group EGW. Neuroendocrine gastroenteropancreatic tumors: ESMO clinical recommendations for diagnosis, treatment and follow-up. *Ann Oncol.* 2008;19(suppl 2):ii104–ii105.
26. Belhocine T, Foidart J, Rigo P, et al. Fluorodeoxyglucose positron emission tomography and somatostatin receptor scintigraphy for diagnosing and staging carcinoid tumours: correlations with the pathological indexes p53 and Ki-67. *Nucl Med Commun.* 2002;23:727–734.
27. Haug AR, Auernhammer CJ, Wangler B, et al. ^{68}Ga-DOTATATE PET/CT for the early prediction of response to somatostatin receptor-mediated radionuclide therapy in patients with well-differentiated neuroendocrine tumors. *J Nucl Med.* 2010;51:1349–1356.
28. Sandström M, Velikyan I, Garske-Roman U, et al. Comparative biodistribution and radiation dosimetry of ^{68}Ga-DOTATOC and ^{68}Ga-DOTATATE in patients with neuroendocrine tumors. *J Nucl Med.* 2013;54:1755–1759.
29. Lubberink M, Direcks W, Emmering J, et al. Validity of simplified 3′-deoxy-3′-[^{18}F]fluorothymidine uptake measures for monitoring response to chemotherapy in locally advanced breast cancer. *Mol Imaging Biol.* 2012;14:777–782.
30. Gunn RN, Sargent PA, Bench CJ, et al. Tracer kinetic modeling of the 5-HT1A receptor ligand [carbonyl-^{11}C]WAY-100635 for PET. *Neuroimage.* 1998;8:426–440.
31. Boellaard R, Oyen WJ, Hoekstra CJ, et al. The Netherlands protocol for standardisation and quantification of FDG whole body PET studies in multi-centre trials. *Eur J Nucl Med Mol Imaging.* 2008;35:2320–2333.
32. Gunn RN, Gunn SR, Cunningham VJ. Positron emission tomography compartmental models. *J Cereb Blood Flow Metab.* 2001;21:635–652.
33. Heidari P, Wehrenberg-Klee E, Habibollahi P, Yokell D, Kulke M, Mahmood U. Free somatostatin receptor fraction predicts the antiproliferative effect of octreotide in a neuroendocrine tumor model: implications for dose optimization. *Cancer Res.* 2013;73:6865–6873.
34. Henze M, Dimitrakopoulou-Strauss A, Milker-Zabel S, et al. Characterization of ^{68}Ga-DOTA-D-Phe1-Tyr3-octreotide kinetics in patients with meningiomas. *J Nucl Med.* 2005;46:763–769.
35. Koukouraki S, Strauss LG, Georgoulias V, Eisenhut M, Haberkorn U, Dimitrakopoulou-Strauss A. Comparison of the pharmacokinetics of ^{68}Ga-DOTA-TOC and [^{18}F]FDG in patients with metastatic neuroendocrine tumours scheduled for ^{90}Y-DOTATOC therapy. *Eur J Nucl Med Mol Imaging.* 2006;33:1115–1122.
36. Koukouraki S, Strauss LG, Georgoulias V, et al. Evaluation of the pharmacokinetics of ^{68}Ga-DOTATOC in patients with metastatic neuroendocrine tumours scheduled for ^{90}Y-DOTATOC therapy. *Eur J Nucl Med Mol Imaging.* 2006;33:460–466.
37. Patlak CS, Blasberg RG, Fenstermacher JD. Graphical evaluation of blood-to-brain transfer constants from multiple-time uptake data. *J Cereb Blood Flow Metab.* 1983;3:1–7.
38. Gunn RN, Lammertsma AA, Hume SP, Cunningham VJ. Parametric imaging of ligand-receptor binding in PET using a simplified reference region model. *Neuroimage.* 1997;6:279–287.
39. Watabe H, Jino H, Kawachi N, et al. Parametric imaging of myocardial blood flow with ^{15}O-water and PET using the basis function method. *J Nucl Med.* 2005;46:1219–1224.
40. Patlak CS, Blasberg RG. Graphical evaluation of blood-to-brain transfer constants from multiple-time uptake data: generalizations. *J Cereb Blood Flow Metab.* 1985;5:584–590.
41. Kratochwil C, Stefanova M, Mavriopoulou E, et al. SUV of [^{68}Ga]DOTATOC-PET/CT predicts response probability of PRRT in neuroendocrine tumors. *Mol Imaging Biol.* 2015;17:313–318.
42. Öksüz MO, Winter L, Pfannenberg C, et al. Peptide receptor radionuclide therapy of neuroendocrine tumors with ^{90}Y-DOTATOC: is treatment response predictable by pre-therapeutic uptake of ^{68}Ga-DOTATOC? *Diagn Interv Imaging.* 2014;95:289–300.
43. Velikyan I, Sundin A, Eriksson B, et al. In vivo binding of [^{68}Ga]-DOTATOC to somatostatin receptors in neuroendocrine tumours: impact of peptide mass. *Nucl Med Biol.* 2010;37:265–275.
44. Harms HJ, Knaapen P, de Haan S, Halbmeijer R, Lammertsma AA, Lubberink M. Automatic generation of absolute myocardial blood flow images using [^{15}O]H2O and a clinical PET/CT scanner. *Eur J Nucl Med Mol Imaging.* 2011;38:930–939.